Journal of Molecular Liquids 335 (2021) 116151

Contents lists available at ScienceDirect

Journal of Molecular Liquids

journal homepage: www.elsevier.com/locate/molliq

Frequency-responsive cooperativity of graphene oxide complexes under a low AC bulk electric field

Kyongok Kang [a,*], Dongwook Lee [b], Jiwon Seo [b,*]

[a] Forschungszentrum Jülich, Institute of Biological Information Processing, Biomacromolecular Systems and Processes (IBI-4), 52425 Jülich, Germany
[b] College of Science and Technology, Department of Physics, Yonsei University, 1 Yonseidae-gil, Wonju-si, Gangwon-do 26493, Republic of Korea

ARTICLE INFO

Article history:
Received 27 October 2020
Revised 6 April 2021
Accepted 10 April 2021
Available online 17 April 2021

Keywords:
Graphene oxide
Frequency-responsive reorientations
Cooperativity of GO-complexes
In-situ electric field dynamic light scattering
Image-time correlation

ABSTRACT

Graphene oxide (GO) is a promising material for the construction of biological functional surfaces and corresponding biomedical applications. The physical properties of sheets of GO are determined by its conductivity, flexibility (being just a few atomic carbon layers thick), and hydrophilicity/hydrophobicity. In order to exploiting multitask surfaces, however, controlling reliable tunability of the complex formation with other macromolecules in aqueous environments is highly non-trivial due to the hydrophobic nature of GO. Thus, one effective way of complicated physical process of dealing with aqueous systems of GO is to perform the complex formation under *in-situ* external fields. In this paper, we report the response of GO-sheets, complexed with spherical colloidal polystyrene particles, nafion, and long and thin DNA-viruses (fd), in alternating electric fields, probed by means of novel experimental methods of image-time correlation spectroscopy and small-angle dynamic light scattering. Here, the frequency-responsive reorientations of a GO-sheet are interpreted by random orientations of particles. As results, we have found that GO carries overall local reorientations with feedback oscillations, as well in the GO-complexes (of a colloidal sphere polymerized polystyrene (PPs) and nafion solution). However, such oscillations are absent, as overdamped Brownian motion, in the mixture of DNA-virus suspension (with GO-PPs). This indicates that Brownian fluctuations of GO can be effectively stabilized, and cooperated in the membrane-based, isotropic rod-mesh network of DNA-virus (fd) suspension. We hope then the results are useful to foster better designs of processing GO-sheets in the controls of accessible biological and biomedical applications.

1. Introduction

The application of graphene and graphene-based materials have been greatly interested in various research fields due to their excellent properties on the linear dispersion, the mobility with a high surface area [1–4], and used for the single-molecule gas detection (chemical sensors), optoelectronic devices, magnetic properties, and energy storage [5–15]. Graphene is a 0.14 nm thick layer of carbon atoms bonded through two-dimensional sp2 hybridization. Among graphene-based materials, graphene oxide (GO) is one of the attractive systems in its multiple potential applications, based on the composition of *two regions*: *graphitic and non-graphitic* [5,16–19], where the graphitic regions are dispersed in the non-graphitic regions, while the graphitic domains act as small graphene islands. Also, these graphitic domains illustrate quantum characteristics, mimicking photoluminescence emission originated by the quantum confinement effect [10,20–21]. Moreover, the graphitic regions are hydrophobic (apolar), while the non-graphitic regions are hydrophilic (polar), providing amphiphilicity to GO [22–23]. Thus, non-uniform charge distribution on the surface of GO is commonly occurred in the mixing process of graphitic and non-graphitic regions, which then varies the polarization effect. Furthermore, depending on the temperature and frequency of an alternating electric field, the redistribution of charge surrounding of GO (with its high dielectric constant) can be accessible by apparent amphiphilicity changes of the "space charge" behaviors [24]. Such amphiphilicity of GO is already well adapted in the use of liquid crystal display (LCD) applications, controlled by a DC voltage, carrying the specific motion and rotation of GO [25–29]. Although most charged particles respond to an applied external electric field, rarely few particle systems show response in an alternating

Abbreviations: CCR2, CC chemokine receptor 2; CCL2, CC chemokine ligand 2; CCR5, CC chemokine receptor 5; TLC, thin layer chromatography.

* Corresponding authors.
E-mail addresses: k.kang@fz-juelich.de (K. Kang), jiwonseo@yonsei.ac.kr (J. Seo).

https://doi.org/10.1016/j.molliq.2021.116151
0167-7322/

electric field with some resonant frequencies, which is known as the dynamic properties that are selectively triggered by an AC field. Such dynamic control is essential in the case of microfluidics, in particular, for utilizing the amphiphilicity and the surface potential of GO in the biomedical fields. There, it is also important to investigate the properties of GO depending on the relations to the degree of oxidation, pH of the solution, and its effective volume in the solvent [30–31]. Thus, before using GO as a drug delivery agent, the validity of the biomedical application with other various pharmaceutical substances is surely left as crucial challenges, for dealing with the interacting substances of the surface of GO via specific amphiphilicity [32–33]. However, up to now, the motion of GO in bulk solvents and the control of the fluidic behaviors have not yet been fully explored due to the difficulty of either detection or control in the bulk and confined geometries (of microfluidics). Furthermore, the task of controlling "transport" or "cargo" delivery requires delicate maneuvering the rotational and translational motion of GO, with rigorously "triggered" for specific (i.e., pharmaceutical) elements to a certain "targeted" position. Therefore, it is worthwhile to explore field-induced responses of GO in bulk solutions and to visualize the electric polarization effect, for exploiting the rotational motion of GO via low external electric fields.

When the system is under an external field, the particles (or colloids) respond either to attract or repel, depending on the interaction potential. We address, here, briefly the dynamical motions, known as "electric polarization" [34], by the modified Smoluchowski equation (MSE) for the average of orientations of particles. This then implements the probability of orientation functions relating to the results on the frequency-responsive microscopic dynamics of GO and GO-complexes in the mean-field averages. The systems are explored for both freely rotating graphene oxide (GO) sheet (size: 4 μm), by the image-time correlations, and the diluted GO-dispersed solution with other mixtures (at a low-ionic-strength of 0.032 mM Tris/HCl buffer solution), under an in-situ electric field small angle dynamic light scattering. *As a highlight of the interest for the feasibility of GO employed to a functional biomaterial, GO-complex mixture is demonstrated by the DNA-viruses (fd), and shown in the* Scheme 1. The possible cooperativity of DNA strand-loaded GO, is briefly illustrated in Scheme 1, as a GO-complex template interacting with a target cell, where its rotational force mimics a "molecular drill" in the membrane fluctuations. This may bring useful impacts to other applications of GO, for both fundamental understanding of amphiphilicity of GO, and engineering in field-controlled narrow channel flows. Therefore, it is our motivation, in this paper, to demonstrate the frequency feedback responses of GO, as well in the electric polarization of GO-complexes for their variable "transport" behaviors.

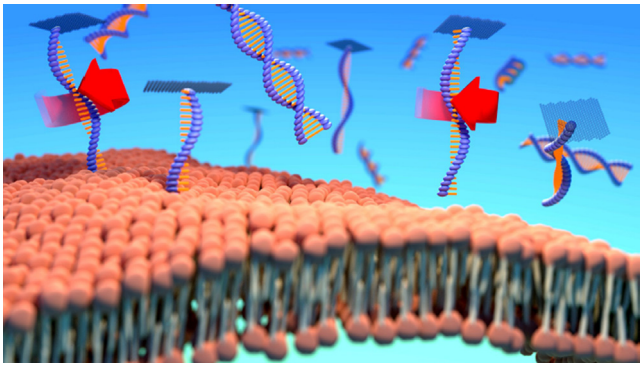

Scheme 1. A schematic of DNA strand-loaded graphene oxide (upper part) showing its high efficacy in entering a target cell due to its rotational motion, mimicking a" molecular" drill in the membrane (lower part) fluctuations.

The paper is organized as follows: we introduce the experimental methods of both image- and signal-processing, with the sample preparations, followed by the principles of electric polarization (described by modified Smoluchowski equation). As experimental results, the frequency responses of GO and GO-complexes are discussed: (i) First, the observation of local orientation changes of a GO sheet (size: 4 μm) in solvent are shown, under a low-amplitude AC (sinusoidal wave) electric field, for two distinguishable frequencies, at a low- (10 Hz) and a high-frequency (1 kHz), both in the real- and Fourier space. In the absence of an electric-field and a low-frequency, relatively free rotations of GO-sheet are observed. On the contrary, the "restricted" orientations are seen at a high frequency. (ii) Second, the image-time correlations are performed (at the Fourier space) for the frequencies depicting averaged orientational motions of the GO-sheet. (iii) Third, the accessibility of GO- complexes with other particles (as polymerized polystyrene colloidal sphere, nafion solution, and DNA-virus suspensions) are provided for exhibiting variations of microscopic dynamics, measured by an *in-situ* small angle electric-field dynamic light scattering (SAeDLS). Finally, the conclusion is drawn for frequency-responsive averaged orientations of GO that are discussed with both translational and rotational microscopic cooperativity of GO-complex mixtures.

2. Experimental methods and sample preparation

To probe proper frequency-responsive feedbacks of both orientation changes and microscopic relaxations dynamics of GO- and GO-complexes, here, two novel experimental methods are employed; one is the image-time correlation and the other is small angle dynamic light scattering are, under an *in-situ* AC electric field. Fig. 1(a) shows the real view of a home-made optically transparent electrical cell, placed under an inverted optical microscope, in two parallel indium-tin-oxide (ITO) glass substrates with a separation of 1 mm. The detail scheme of an in-situ eclectic cell (for the optical microscopy) is in Fig. 1(b), with commercially available custom-designed ITO-coated float glass (obtained from Präzisions Glas und Optik GmbH, CEC500S) with the dimensions of 40×70 mm^2 and a thickness of 0.7 mm. The ITO layer has a high visible-light transmission (90%) at 633 nm and a coating thickness of 15 nm. The sample (400 μL) was loaded on the bottom plate inside a rectangular insulating PTFE film spacer (Armbrecht and Matthes GmbH, AR5038 and AR5038GP) with a thickness of 1 mm. The upper electrode was then gently placed on the lower plate. Due to the capillary forces, the sample droplet adopts a circular form, whose diameter is typically 18–19 mm. The real view of a small-angle electric-field dynamic light scattering (SAeDLS) is shown in Fig. 1(c), where the laser beam is vertically aligned though the sample stage in the middle (as the yellow line).

The sample is loaded inside two plates, sealed by using the PTFE tape to avoid any evaporation of the sample and fixate the two electrodes. All measurements were performed at the center of the sample to ensure a homogeneous electric field. The ITO layers were then connected to a function generator (Avtech model AV-151G-B, 1 Hz–350 kHz, maximum 200 V, load resistance $\geq$ 50 kΩ) via electronic connection pins. A sinusoidally varying electric potential was applied to the electrodes. Here, the electrode polarization is taken care to treat the true bulk electric field, in the middle (see Fig. 2(a)), away from building up arbitrary charges on the ITO glass substrates.

The measurement of collective microscopic relaxation dynamics of GO- and its GO-complexes, are done by a homebuilt small angle electric-field dynamic light scattering (SAeDLS), for both polarized- (VV-mode) and depolarized (VH-mode) scattering. Here, the wavelength of the He-Ne laser light is 633 nm (JDS Uniphase

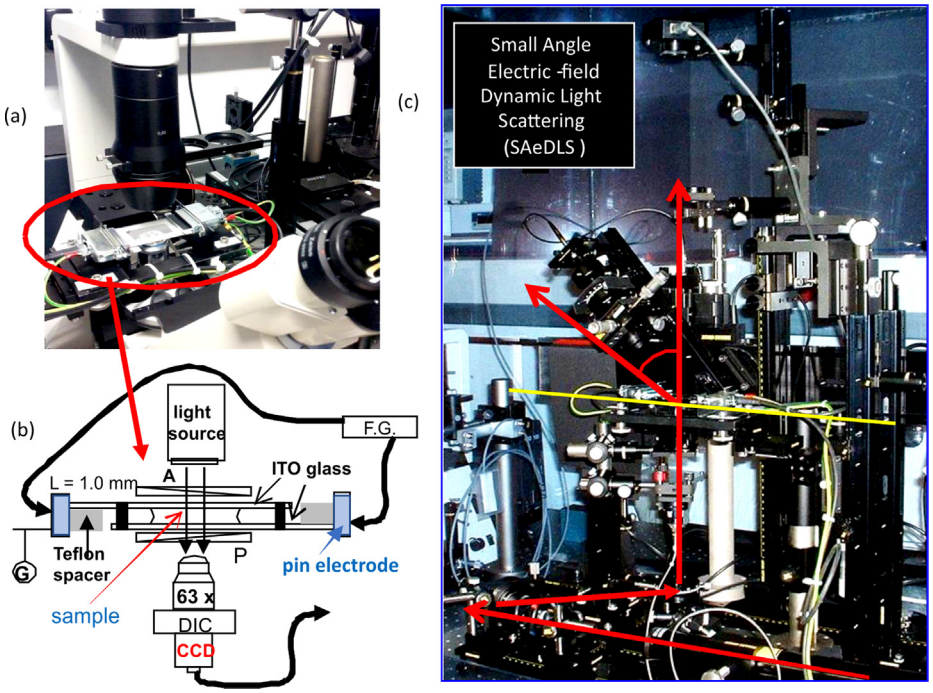

Fig. 1. (a) The experimental setup of an *in-situ* electrical cell under an inverted microscope and (b) detail scheme of an electro-optic cell for the microscopy, under depolarized light. (c) A real view of the small angle electric-field dynamic light scattering (SAeDLS) setup, where the AC electric field is applied to the vertical and as the parallel direction to the incident laser beam (indicated as the red arrow bar). Here the scattering wavevecotr is in the range of 1.8–4 μm of the bulk scattering geometries.

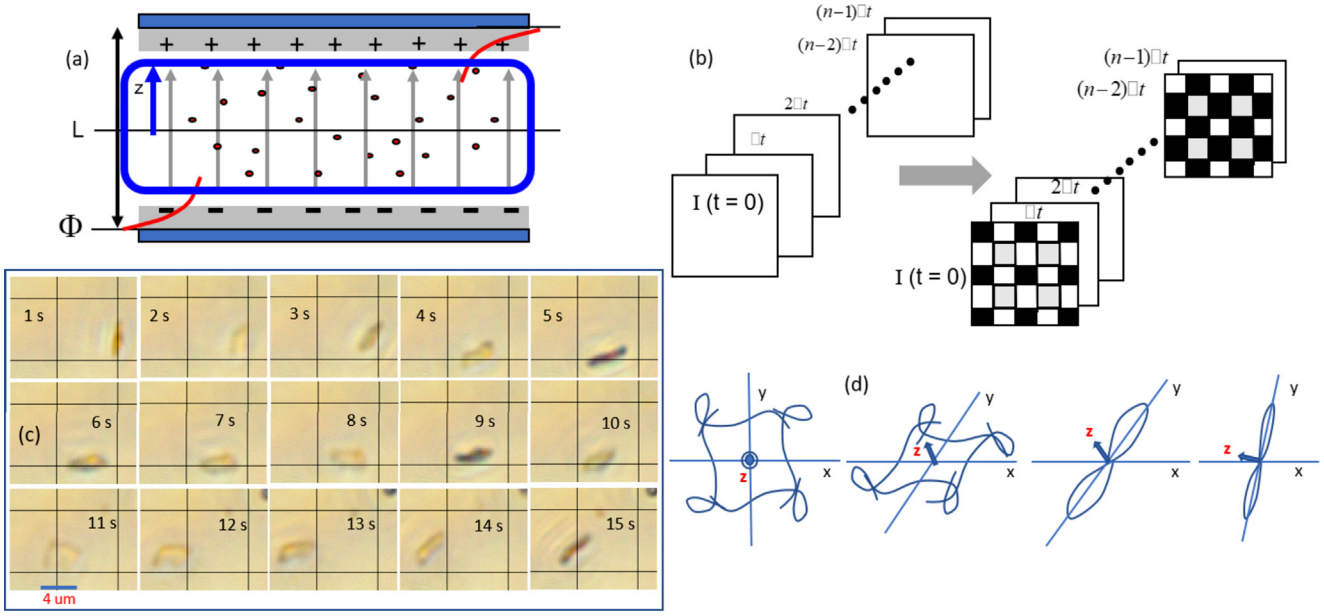

Fig. 2. (a) A simple scheme of electrode polarization layer (decays from the electric potential ∅) and the bulk electric field (of the amplitude of 10 V/mm), in the middle of electro-optic cell thickness L (b) A brief illustration of image-time correlation spectroscopy, (c) Low-frequency (10 Hz)-controlled spatial–temporal images of a graphene oxide (GO) sheet. Note that there are no shape deformations; instead, different orientations of rotational motions are present in both the absence and presence of a low-frequency electric field. Bulk free rotations of the GO sheet (size: 4 μm) in a low ionic-strength (0.032 mM) Tris/HCl buffer solution are shown. The time step is 1 s interval. (d) The possible configurations of GO-sheet at the low-frequency responses, seen in (c).

Model 1145P), and an ALV-5000/EPP multiple tau digital real time correlator is used. Details of the instrumentation of SAeDLS can be found more in the Ref. [35]. Dynamic light scattering correlation functions on suspensions reveal then thermodynamic fluctuations of particles via averaged relaxation times.

The sample preparation are done as follows: GO sample alone was prepared by the Brodie process [5,6], where 5.0 g graphite (99.995% purity, Aldrich) was added to 62.5 mL fuming nitric acid, and then, 25.0 g potassium chlorate was slowly added while the mixture was cooled in an ice bath. After the mixture reached room temperature, it was slowly heated again to 45 °C and maintained for 20 h. The mixture was then poured into 125 mL cold distilled water and heated to 70 °C. After centrifugation at 5000 rpm, the mixture was dried overnight at 70 °C.

Subsequently, brown graphite oxide powder was obtained. The reaction was repeated with fuming nitric acid, and the powder turned into yellow GO. After centrifugation, the powder was finally dried at 70 °C. In the current experiment, GO powder was mixed with water and redispersed in a Tris/HCl buffer solution with a low (0.032 mM) ionic strength.

For the GO-complex mixtures, three different systems are chosen: (i) First is polymerized PS microspheres (PPs), prepared by dispersion of purified styrene monomer, with polyvinylpyrrolidone (molecular weight Mw ~ 55 Kg/mol), 2-azobisisobutyronitrile, and ethanol used as a stabilizer, initiator, and dispersion medium, respectively [36]. The diameter of PPs is 1.5 μm, and negatively charged, dispersed in a low ionic strength (0.032 mM) Tris-HCl buffer. (ii) Second is nafion solution, purchased from Dupont-D1021 Nafion ®, Ion Power GmbH (Terminalst, Mitte. 18, Level 5), as an efficient ion exchange material that is typically used for the fuel cell and membrane technology, containing small portion of a metallic (platinum) dispersed in water. Then, hydrogen gas is expected to generate, acts as the biding agent via the gas diffusion layers. However, in this work, the nafion solution is only used for the mixture with diluted GO (as 1:1 mixing). (iii) Third, DNA-solution is employed for an isotropic-phase of a very low ionic strength (0.032 mM Tris/HCl buffer) fd-virus suspension (in the concentration of 0.5 mg/ml). DNA-virus, bacteriophage fd-virus particles are highly charged (a total charge of 9600 elementary charges), consisting of a helical DNA strand, covered with about 2700 coat proteins [37]. The length of a fd-virus particle is 880 nm, and the core thickness is 6.8 nm. The persistence length is about 2200–2500 nm, with a relatively large Debye screening length of 54 nm for the given ionic strength (of 0.032 mM Tris/HCl buffer solution) [38].

The measurement of bare optical morphologies, is then collected by using a bright-field microscope under an *in-situ* electric field. Typically, a large size distribution of the GO sheets is observed. Here, we have focused an interest of a 4 μm sized GO sheet that dispersed in the low-ionic-strength Tris/HCl buffer solution; the freely rotating oriented GO sheet is observed, in response to an applied external electric field in bulk. The orientation of GO-sheet changes relatively fast (within 0.5 s), exhibiting multi-axis rotations, shown in Fig. 2(d), with different orientational configurations. A test particle (of a 1.5 μm sized polymerized polystyrene (PS) sphere) is seen, as a tracer, in the Tris/HCl buffer solution. The images are obtained using an inverted microscope (Carl Zeiss, Axiovert 40CFL model), under a 63X objective lens (0.75 Korr LD Plan-Neofluar), and the region of interest was about 143 μm × 111 μm, equipped with a CCD camera (AxioCam Color A12-312, 1300 × 1030 pixels) in the polarization mode along with a differential interference contrast microscope. The brief scheme of an image-time correlation spectroscopy is illustrated in Fig. 2(b), with the phase-contrasted images in Fig. 2(c). Fig. 2(d) shows few examples of the possible such orientation configurations of the GO-sheet, for their continuous rotations in real-space.

3. Theoretical background of ensemble average of orientations by modified smoluchoswski equations

The rotational motion of a Brownian object can be described, in principle, by a Modified Smoluchowski equation (MSE); when the polar or anisotropically polarizable molecules rotate in a plane [34], with an orientational distinction function $f(\theta,t)$, and an azimuthal angel θ and time t (represented in Fig. 3), then the equation of motion can be described as

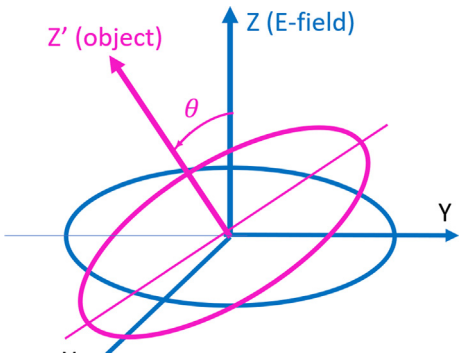

Fig. 3. The simple Euler angular presentation of the orientations of a Brownian object in an electric field $E(t)$.

$$\frac{\partial^2 f(\theta,t)}{\partial^2 t}+\frac{\xi}{I}\frac{\partial f(\theta,t)}{\partial t}=\frac{1}{\sin\theta}\frac{\partial}{\partial\theta}(\sin\theta)\left[\frac{1}{I}f(\theta,t)\frac{\partial W}{\partial t}+\frac{kT}{I}\frac{\partial f(\theta,t)}{\partial t}\right], \tag{1}$$

where I,ξ, and kT corresponds to the moment of inertia, rotational friction, and the thermal energy (in room T), respectively. If the orientation potential energy of a particular object $W(\theta)$, is expressed by the composition of both permanent dipole moment μ and the induced dipole moment $\Delta\alpha$, for an applied electric field $E(t)$, then

$$W(\theta)=-\mu E(t)\ \cos\theta-\frac{1}{2}\Delta\alpha\ E^2(t)\cos^2\theta \tag{2}$$

The time-ensemble averaged orientation function is also estimated by, in general, as the *n-th* Legendre polynomial, where $n=1,2,3,\cdots$ is the integer index (but in the practice, it truncates up to 2nd order, $n=2$), as

$$\langle P_n(\cos\theta)\rangle(t)=\int_0^{\pi}P_n(\cos\theta)f(\theta,t)\sin\theta d\theta \tag{3}$$

By multiplying the *n-th* Legendre polynomials to the Second Differential Equation (SDE) of the orientational distribution function (Eq. (1)), and integrating form 0 to π, then it gives [34]

$$\begin{aligned}&\tfrac{I}{kT}\left\langle\tfrac{d^2P_n(u)}{dt^2}\right\rangle(t)+\tfrac{1}{D}\left\langle\tfrac{dP_n(u)}{dt}\right\rangle(t)+n\ (n+1)\langle P_n(u)\rangle(t)\\&\quad=\gamma(t)\ \tfrac{n(n+1)}{2n+1}[\langle P_{n-1}(u)\rangle(t)-\langle P_{n+1}(u)\rangle(t)]\\&+\beta(t)\ \tfrac{n(n+1)}{2n+1}\left[\tfrac{2n+1}{(2n-1)(2n+3)}\langle P_n(u)\rangle(t)+\tfrac{n-1}{2n-1}\langle P_{n-2}(u)\rangle(t)-\tfrac{n+2}{2n+3}\langle P_{n+2}(u)\rangle(t)\right]\end{aligned} \tag{4}$$

where $\gamma(t)=(\mu/kT)\ E(t)$,and $\beta(t)=(\Delta\alpha/kT)\ E^2(t)$.

In the case of a negligible inertia, then $I=0$ in Eq. (4). The electric-polarization is proportional to the ensemble average of $\langle P_1(u)\rangle(\tau)$, with the reduced variable as $\tau D^{-}t$, with a rotational diffusion D, as

$$\begin{aligned}&\tfrac{d}{d\tau}\langle P_n(u)\rangle(\tau)=-n(n+1)\left[1-\tfrac{\beta(\tau)}{(2n-1)(2n+3)}\right]\langle P_n(u)\rangle(\tau)\\&\quad+\gamma(\tau)\ \tfrac{n(n+1)}{2n+1}[\langle P_{n-1}(u)\rangle(\tau)-\langle P_{n+1}(u)\rangle(\tau)]\\&+\beta(\tau)\ \left[\tfrac{(n-1)n\ \ (n+1)}{(2n-1)(2n+1)}\langle P_{n-2}(u)\rangle(\tau)-\tfrac{n\ \ (n+1)(n+2)}{(2n+1)(2n+3)}\langle P_{n+2}(u)\rangle(\tau)\right]\end{aligned} \tag{5}$$

Here, by taking only dominant terms in the contribution of an electric field, then

$$\begin{aligned}\langle P_1(u)\rangle(\tau)&=\textstyle\int_{-\infty}^{\tau}d\tau'\exp\left(-2\int_{\tau'}^{\tau}\left[1-\frac{\beta(\tau_1)}{5}\right]d\tau_1\right)\left\{\tfrac{2}{3}\gamma(\tau')[1-\langle P_2(u)\rangle(\tau')]\right\}\\&=\textstyle\int_{-\infty}^{\tau}d\tau'\exp(-2(t-\tau'))\left[1+\frac{2}{5}\int_{\tau'}^{\tau}\beta(\tau_1)d\tau_1\right]\left\{\tfrac{2}{3}\gamma(\tau')[1-\langle P_2(u)\rangle(\tau')]\right\}\end{aligned} \tag{6}$$

where

$$\beta(\tau)=\frac{\Delta\alpha}{kT}\left[E_C^2+2E_CE_O\cos(\omega' t)+\frac{1}{2}E_O^2(1+\cos(2\omega' t))\right] \tag{7}$$

and the frequency is scaled as $\omega' = \omega/D$

$$\langle P_1(u)\rangle(\tau) = \frac{2}{3}\int_{-\infty}^{\tau} d\tau' e^{-2(\tau-\tau')} \left\{ 1 + \frac{2}{5}\left[\begin{array}{l} \left(\frac{\beta_O}{2} + \beta_C\right)(\tau - \tau') \\ +\beta_{OC}\frac{\sin(\omega'\tau)-\sin(\omega'\tau')}{\omega'} \\ +\frac{\beta_O}{2}\frac{\sin(2\omega'\tau)-\sin(2\omega'\tau')}{2\omega'} \end{array} \right] \right\} * \gamma(\tau')[1 - \langle P_2(u)\rangle(\tau')] \tag{8}$$

where

$$\beta_O = \frac{\Delta\alpha}{kT}E_O^2, \quad \beta_C = \frac{\Delta\alpha}{kT}E_C^2, \quad \beta_{OC} = \frac{\Delta\alpha}{kT}(2E_OE_C) \tag{9}$$

Here, "o" indicates for the "oscillating" and "c" for "constant" term, with

$$\gamma(\tau) = \frac{\mu}{kT}E_C + \frac{\mu}{kT}E_O\cos(\omega'\tau) = \gamma_C + \gamma_O\cos(\omega'\tau) \tag{10}$$

The last term on the right side of Eq. (8) contains the ensemble average of a second Legendre polynomial that is known as the electric birefringence [34], expressed as

$$\langle P_2(u)\rangle(\tau) = \frac{4}{5}\int_{-\infty}^{\tau} d\tau_1 \int_{-\infty}^{\tau_1} d\tau' \quad e^{-6(\tau-\tau')}\gamma(\tau')e^{-2(\tau-\tau_1)}\gamma(\tau_1) + \frac{2}{5}\int_{-\infty}^{\tau_1} d\tau' \quad e^{-6(\tau-\tau')}\beta(\tau') \tag{11}$$

and the linearized form of electric polarization is as $\langle P_1(u)\rangle_L(\tau) = \frac{2}{3}\int_{-\infty}^{\tau} d\tau' e^{-2(\tau-\tau')}\gamma(\tau')$.

The electric polarization of the complex variable, $\boldsymbol{P}(\omega) = P'(\omega) - P''(\omega)$, is then obtained by applying the Laplace transform to Eq. (8), known as the Cole-Cole diagram [34].

Note that the reduced time τ' (above) is a dummy variable in the decay exponent function, as a time propagator with the retardation 2(t-τ'). To implement these mathematical descriptions, here, the interplay between the reduced variable of "$\tau D^{-}t$" and the frequency-driven effective rotational frictions, $\omega' = \omega/D$ is considered. Then, the diffusion constant is, conveniently, an "implicit" parameter in the frequency-responsive electric polarization for ensemble average of orientations (as $\omega'\tau\ \omega t$). In this work, the relations between mesoscopic frequency–response time and microscopic relaxations are probed, respectively, by the image-time correlation and small-angle dynamic light scatterings. As it can be seen our results, in the following section, the "tunings" of GO are feasible under low AC electric fields; by either "oscillating" motion (of particles) or the "overdamped" Brownian motions of GO in the membrane-based open rod-network (of DNA-viruses (fd)).

4. Results and discussion

4.1. Frequency-dependent orientations of the GO sheet and electric polarizations

A freely rotating GO sheet (size: 4 μm) is observed at a low-frequency of 10 Hz (and a field amplitude of 10 V/mm), under a microscope, shown in Fig. 4(a), where the temporal morphology is revealed by the "reorientation" of a GO-sheet. At a fixed time-lapsed image, the GO-sheet may seem to be deformed, but actually it reorients continuously with rotations. This can be seen clearly in the supplementary data Movie A provided in Fig. 4(a).

In contrast, at a high frequency (above a few kHz), only slight changes in the orientations of the GO-sheet are observed as the "constrained" rotational motions in Fig. 4(b). Also, intriguingly, the bare optical morphology of bright-field images of GO-sheet shows a "color" effect, due to locally different refractive indices of the GO-sheet in some configurations (see the brightfield images in Fig. 2(c)). This originates from the slight changes in orientations, observed as the rotational motion of a GO-sheet. Further reorientations of the GO-sheet are visualized in the real images of low-frequency driven morphologies, in Fig. 4(a), with the "enhanced" phase-contrasted images, compared to the case of a high-frequency driven orientations, in Fig. 4(b). In an increase of the frequency, from 100 Hz to 1–10 kHz, noticeably "restricted" or "hindered" orientations of the GO-sheet are seen in a narrower orientation distribution configuration (at a high-frequency), resulting "slower" feedbacks of rotational motions. More quantification of such averaged reorientation is determined by the image-time correlation (for the Fourier transformed images), in the following subsection.

4.2. Image-time correlations in Fourier transforms and frequency-dependent feedbacks

To apply image-time correlation functions of the GO-sheet, first Fourier transforms of the real images are obtained for depicting the averaged orientations, at low- and high-frequency-driven bulk electric field, shown in Fig. 5(a) and (b), respectively. Then, the field-controlled rotations of the GO sheet are directly visualized in the Fourier transforms, for representing the averaged orientations of frequency-dependent motions. The averaged orientations are collected in the mesoscopic time binning of 1 s (or 1.25 s). In Fig. 5, the time steps are increased from left to right (and top to bottom). As observed, the repetition of orientations of the GO sheet occurs "faster" at a low frequency (see Fig. 5(a)), on the contrary, at a high frequency, the reorientations occur "slower" (Fig. 5(b)). Thus, the orientation distribution of a GO-sheet, at high frequencies (in the Fourier space) are not much varied in the spatial polarization (in Fig. 5(b)), as compared to the "broader" distributions of low-frequency-driven orientations for the GO sheet (Fig. 5(a)). Such field-induced spatial electric polarization effects are briefly illustrated at each top right-side panel.

The image-time correlation functions are used to extract the quantitative information of "preferred" averaged orientations in time traces, via the intensity transmitted through crossed polarizers in the CCD camera images (with a pixel-pixel indices). To construct an image-time correlation function, the data images have to be reconstructed in time: First, all the time lapsed images (black/white bmp files) ought to be converted as readable 2d Ascii files in the time sequences. Second, the averaged grey intensity < I(t) > is calculated in 2d matrix (i, j) pixel arrays at a given time frame t, with the routing numbers for each raw- and column number indices are i = 0, …, 299, and j = 0, …, 299 for t = 0, .. 299 for the total time frames. Third, the averaged overall pixel intensity is subtracted from an individual 2d pixel array value, and then multiplied by the following time frame binning sequences. Finally, the multiplication of the above intensity is then normalized by the square of the initial time frame values, via home-made integrated program in the Delphi (Lazarus) environment, to calculate the image-time correlation. The very beginning of the image-time correlation starts from 1 and decays in later time, for featuring the characteristic time of changes of morphologies. The black and white pixel intensities are different from the averaged grey pixel intensity $< I(t) >$. Then, the image-time correlation function is defined as

$$C_V(t) = \frac{< (I(t) - < I(t) >)(I(0) - < I(0) >) >}{< (I(0) - < I(0) >)^2 >} \tag{12}$$

where the brackets <···> denote averaging over all CCD-camera pixels. Each single image in a time trace was used to construct an image correlation function, for the region of interest, as in pixels (by 300 × 300 pixels). The above-mentioned definition of the image time correlation function is indicative of the CCD camera pixel intensity correlation function, calculated from the intensity transmitted through two crossed polarizers (instead of PMT (photomul-

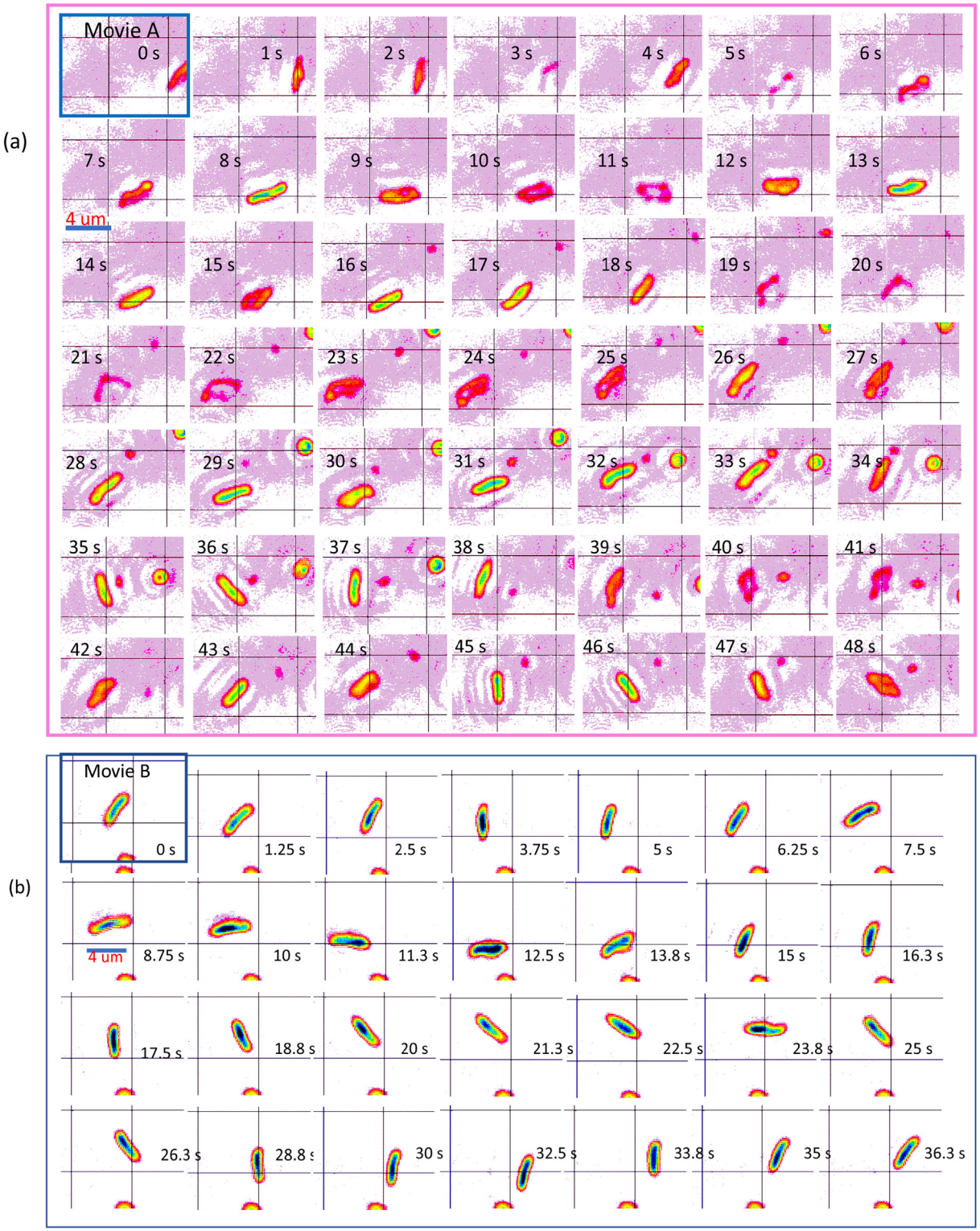

Fig. 4. The "enhanced" phase contrasted images for the orientations and rotations of a GO-sheet at a (a) low-frequency (of 100 Hz) and (b) a high-frequency (10 kHz) controlled spatial–temporal images and its corresponding data movies are shown Movie A and Movie B, respectively. The field amplitude for both frequencies is as 10 V/mm, under AC sinusoidal waveform.

tiplier) scattered intensity detection in light scattering). Here, one should note that the time binning is also flexible to optimize, as well as the initial time frame is chosen as mostly similar to represent the averaged motions of dynamical changes. Then it gives typically a good background of correlation, reaching to the value of 0 (as no correlation in the longer time). Also, the temporal resolution is required as 10–50 times shorter than the repeating cycles of dynamical events. This image-time correlation spectroscopy is originally developed by the needs of investigating the kinetics of field-induced dynamical states of charged DNA-rods, which is well employed in Ref. [39]. More details of the image-time correlation spectroscopy can be found in Ref. [35]. A well-established example

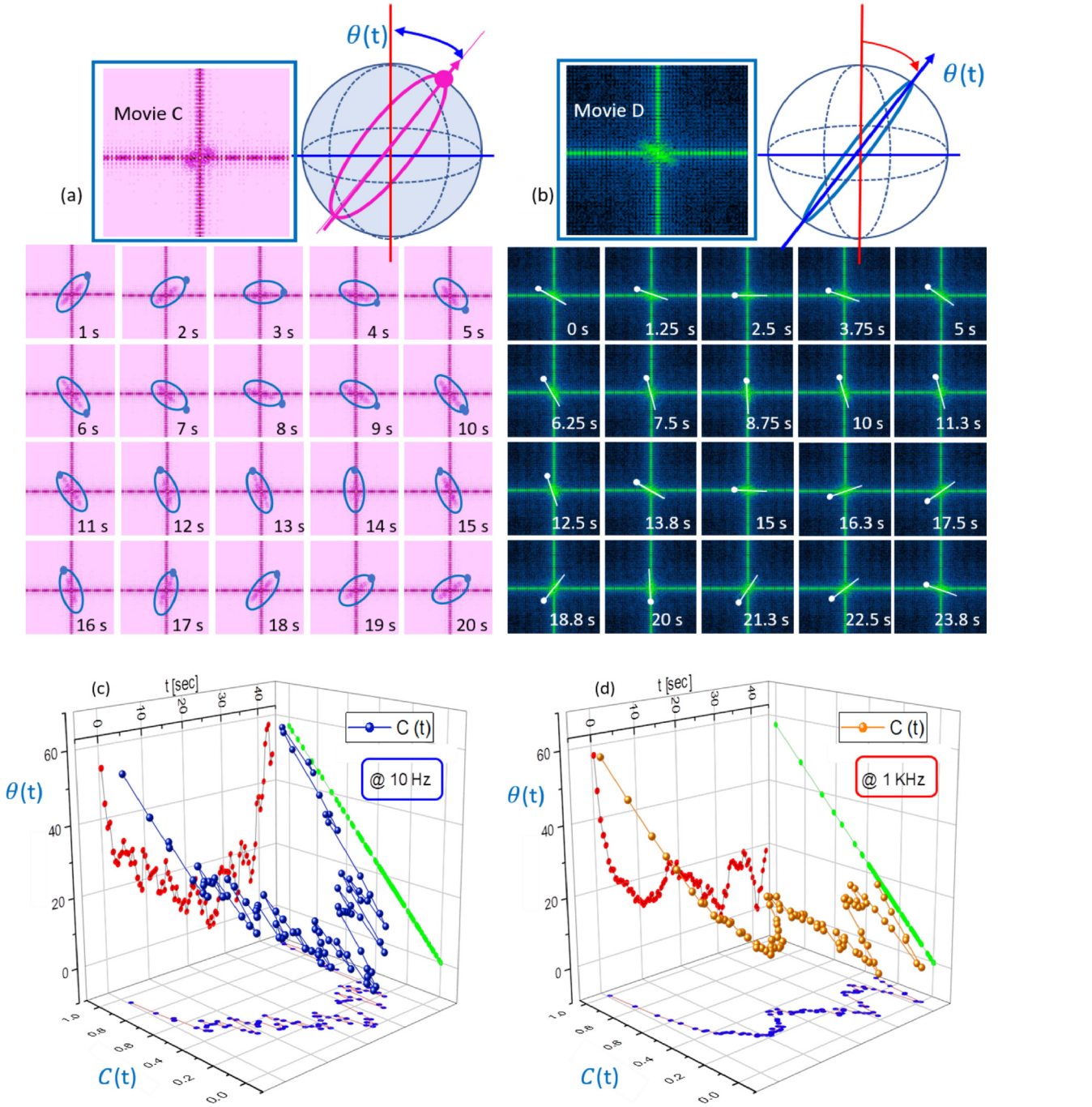

Fig. 5. Fourier transforms of the orientations for (a) a low-frequency rotation (as shown in Fig. 2) and (b) a high-frequency rotation (as shown in Fig. 3). The spatial polarization is depicted at a low- (10 Hz) and a high-frequency (1 kHz), respectively. The whole data flow is run by our home-made integrated program in the Delphi (Lazarus) environment, for given 2d pixel arrays and total time frames. The final outcome of the image-time correlation function is show in (c) and (d), where the correlation function in time is plotted with an additional axis of azimuthal angle of frequency-responsive angle, theta, θ(t) in time. Note that, after 20 s, clearly the "returning" back of orientation occurs at low-frequency response (in c), while only decays at a high-frequency (in d) for the corresponding movie data, Movie C and Movie D, respectively.

of image-time correlations is the electric field-induced dynamical states (with various field amplitudes) in the suspensions of charged rod-DNA strands (fd), exhibiting a field-induced criticality and a "decay rate" or the relaxation for the melting/formation of small nematic domains [35,38,40]. Further applications of image-time correlations are evaluated in different colloidal systems, as slow dynamics of charged DNA-rods in equilibrium [41], polymerized polystyrene dimer oscillations in isotropic-nematic coexistence [42] and local migrations of clay particles [43]. The similar rotational dynamics of nanoparticles are visualized by molecular dynamics simulations [44,45].

In this work, we considered frequency-driven orientational motions of a freely rotating GO sheet (size: 4 μm) dispersed in a low-ionic-strength Tris/HCl buffer solution and exposed to a bulk electric field by image-time correlations. The characteristic features of kinetics for the spatial averages of orientation changes are then obtained by the image-time correlations in the Fourier space.

The result of image-time correlations for frequency-dependent reorientations of the GO-sheet are shown for both low (10 Hz)- and high-frequency (1 kHz) orientations (see the supplementary data of Movie C and Movie D), respectively. Time-lapsed images (bmp files) are collected of presenting the dynamical events of textures, which is converted to the 2d black/white intensity matrices of Ascii files. The pixel size can be varied with an optimization between total numbers of image frames and time binning. Each time frame image intensity values are stored in an Ascii format to calculate pixel-to-pixel correlations at different time frames, normalized by the initial time frame. The whole data flow is run by our home-made integrated program in the Delphi (Lazarus) environment, and the outcome of an image-time correlation function can be seen as the readable Ascii file in the Origin file. Depending on the dynamics of system, the characteristic decay times varies and can be fitted.

More frequent change of rotations is detected at the low frequency, compared to the higher-frequency. Interesting results of the image-time correlations are shown by the difference of frequency-driven feedbacks, in particular, observed after 20 s (on the right side of the region in Fig. 5 (c) and 5 (d)): The low-frequency response of reorientation of a GO-sheet increases, with returning back to an initial orientation. On the contrary, the high-frequency driven orientation decays monotonically from the beginning and "saturates" as the "slower" feedback (see the Fig. 5(d) after 20 s). This supports the rotational or "flipping" motions of the GO-sheet, which is much "hindered" at a higher frequency (~1 kHz). This is due to the electroosmotic flow, compared to the low-frequency (and the absence of an electric field) of the freely-rotating orientations. Thus, frequent change in local orientations of GO-sheet, probed by image-time correlation, is possible for the onset of "distinguishable" frequency-feedbacks rotations of either "free" (at a low-frequency), or the "restricted" (at a high-frequency). These different frequency responses of the rotations are then demonstrated for a single GO-sheet under a low AC electric field in bulk solution (of a 32um Tris/HCl buffer), in which agree with other general observations on the dielectric properties of GO [24,46,47]. Thus, we can say the frequency-dependent dielectric properties of GO are also related with the response function of a dielectric constant depending on the AC frequency, which is described in earlier section. To brief sum up, in the low-frequency regime, GO exhibits a high dielectric constant of the order of $\sim 10^2$ (at room temperature), while in the high-frequency regime (<10 kHz), it exhibits the dielectric constant of below 10, revealing less pronounced space charge polarization. Thus, the rotational motion of GO is influenced by such frequency-controlled polarization effect, apparently well in the GO sheet dispersed at the low-ionic strength bulk solution. Furthermore, the low-frequency induced surface charge modification of GO may causes additional "enhanced" rotational motion. On the contrary, at high frequency, the response of rotational motion is expected to be "reduced", as indeed shown in our result, due to the fact that the electro-osmotic flow is dominant, where the surface charges of GO are not influenced for a large gap of the time-retardance. Electric-field–induced polarization of the layer of condensed ions on cylindrical colloids can be found in Ref. [48].

4.3. Frequency responsive collective modulations of GO-complex mixtures in the in-situ small angle electric field dynamic light scattering (SAeDLS)

Further microscopic relaxation dynamics few GO-complex mixtures are revealed by the frequency responsive collective motions of GO, under an *in-situ* electric field small angle dynamic light scattering (SAeDLS). Much diluted GO-suspension and three GO-complex mixtures are explored for the weak-perturbations of electric-field modulations. The homemade small-angle *in-situ* electric field dynamic light scattering is built to capable probing thermal fluctuations, for both polarized (VV-mode) and depolarized (VH-mode) lights, also designed for anisotropic scattering geometry [35]. Here, the small scattering wavevector is unique, int terms of the scattering wavevector corresponding to the range of submicron to micron length scale, compared to smaller than that of commercially available dynamic light scattering setup [35].As a working example, the mixture of DNA-virus (fd) and polymerized polystyrene (PPs) spheres is well explored in both the absence and presence of an external electric field Ref. [42]. Typical range of the scattering wavevector is used as qL ~ 1–4, where L is the particle length (in micron length). The results of SAeDLS are provided for the comparisons GO-complexes, in the absence of electric field (in Fig. 6), where the visible local oscillation peaks are carried out with "non-negligible" background (at a long-time slow) in the measured intensity auto-correlation functions. Also, there seem to be slightly different scattering volumes, based on the decrease of signal-to noise ratio in the scattered intensity correlation, by an increase of the scattering wavevector (indicated as arrow bars in Figs. 6, 7, and 9). The solid lines are the fits with a single stretched exponent function, as the scattered electric field function, $g\_E(t)\ Aexp(-t/\tau)+B$, where τ is the relaxation time, and A is the amplitude and B is the background. Since the pronounced oscillation peaks are localized in the intensity-correlation function, we disregard them to fit for the simplicity.

As one can see clearly, most pronounced localized oscillation behaviors are present in the GO-PPs mixture (see the Fig. 6 (b)), in the absence of field, which is mainly by the repulsive interactions between GO- and PPs spheres, led by the preparation of PPs particles (see Ref. [42]) that polystyrene spheres are uniformly coated with the negatively charged polymers. In the presence of an electric field (at a frequency of 100 Hz and a moderately low field-amplitude of 2 V/mm), these local oscillations of GO-PPs mixtures become reduced, but still visible, with similar relaxations, in the scattering amplitude fluctuations, in Fig. 7(b). However, such localized oscillations are completely absent in the mixture of GO-PPs-(iso) fdVs (see the Fig. 6(d)), shown as the "overdamped" Brownian motion. Note that these enhanced oscillations of GO-PPs are completely overdamped in the mixture of isotropic-phase of DNA-virus (fd) suspension, even in the absence of an electric field. This strongly supports the possibility of DNA-virus suspensions that are embedded "cooperatively" well with the GO-PPs mixture, in the open-meshwork of an isotropic phase of charged DNA-rods (at the low ionic strength of Tris/HCl buffer solution). Also, these overdamped motions are seen in various applied electric-field conditions, in Fig. 7(d), for depicting the possible dispersion relations of GO as exhibiting to the stabilized Brownian motion.

Qualitatively similar oscillation peaks are found in the case of GO-nafion complex, contributing to the scattering amplitude at long-time tail modulations (after 10 sec), in Fig. 6(c) and Fig. 7 (c). Note that the typical electric-field strengths (that we apply) in the present study (<2 V/mm) are weak enough to induce only a slight perturbation to the system of GO and GO-complexes, without causing any indication of the electroosmotic flows. The slow time modulations sustain the "non-vanishing" background oscillations (in the few tens of sec), in the long-time correlation function, under a weak electric field. Fig. 8 is the residual fits for the comparison of intensity auto-correlation function in the background oscillations (for the suspension of a diluted GO), without- and with-an electric field. The slow time oscillation feedback of GO itself is, however, not negligible, at far low-frequency (in the range of 100 mHz), relating to somewhat "intrinsic" electric polarization. Furthermore, this coincides with a high amplitude of non-negligible oscillatory fluctuation, as slow time tails (of 10 s) in

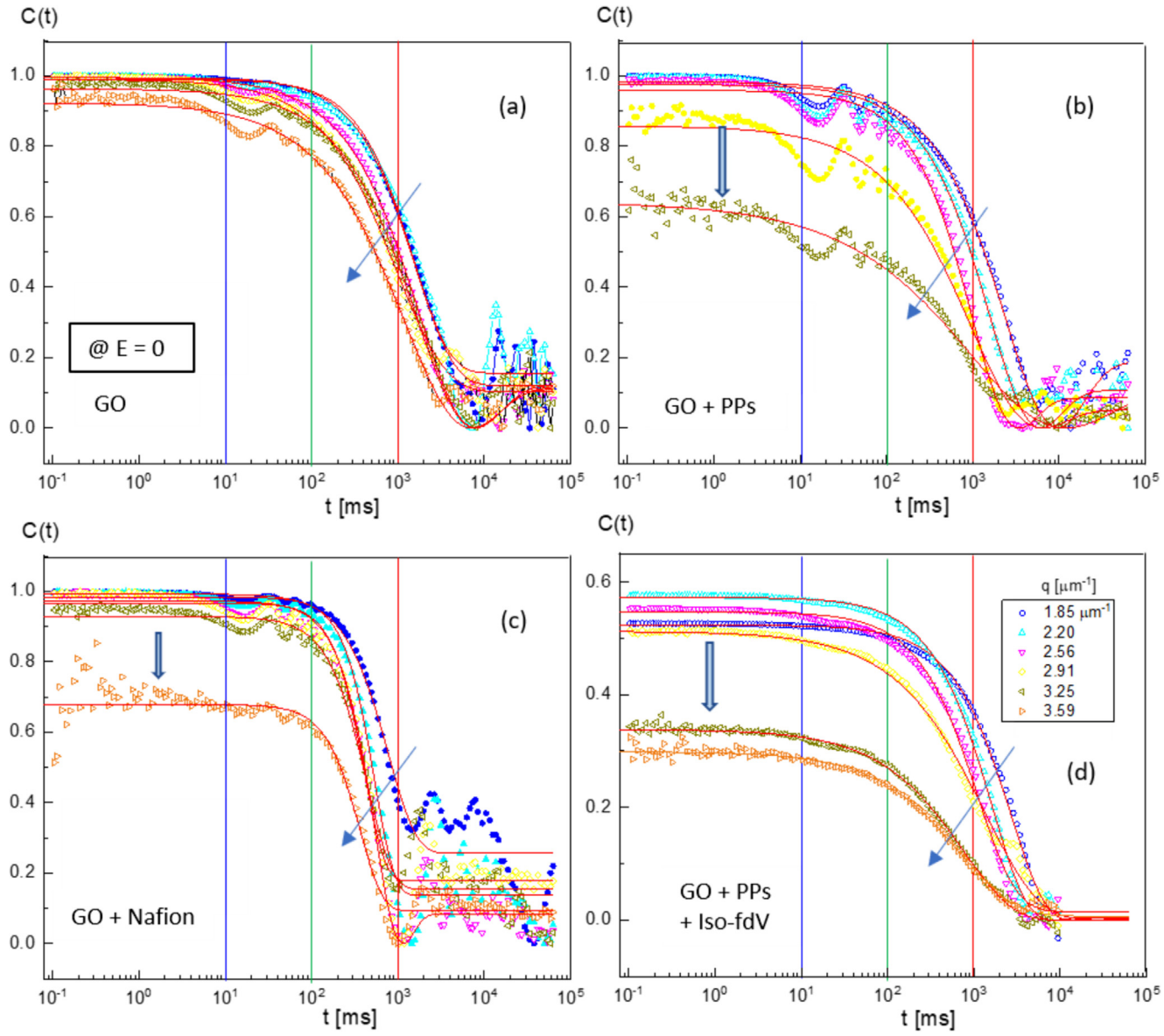

Fig. 6. Intensity auto correlation functions in the small-angle dynamic (polarized) light scattering, in the absence of an electric field for few small wavevectors (indicated an arrow for the increase of wavevector q): (a) for a diluted GO-mixture, (b) GO-PPs mixture, (c) GO-Nafion mixture, and (d) GO-PPs and isotropic DNA-virus suspension. Apparent local oscillations are shown in the time window of 10–100 ms and slower time tails, except the GO-PPs-(iso) fdVs in (d). The solid lines are the fit by a single exponent stretched function, with neglecting the local oscillations (in which the summary of relaxation rates is listed in Table 1). The relative signal to noise ratio of a correlation function decreases (indicated as the left vertical down arrow), in an increase of the wavevector q.

the correlation functions, under an electric-field, disregard of longer-time duration measurements.

Table 1 is the summary of relaxation rates, obtained from the scattered intensity auto-correlation functions (shown in Fig. 6 and Fig. 7) that are fitted by a single stretched exponent function. The quantity is then the collective relaxations of thermal fluctuations of GO-complex mixtures, for given small scattering wavevectors. The apparent local oscillations are disregard here, due to their localization at the same low-frequency (of 10–100 Hz).

Although such local oscillations can be fitted, in the case of the drift-velocity existing for particles with a phase shift retardance (for a scattering wavevecor q), this is left beyond the scope of this paper. We have found that, in Table 1, much small values of the relaxation rates, $\Gamma \sim 1/\tau\,[s^{-1}]$ are shown, compared to typical relaxations of colloidal particle, both in absence and presence of a low frequency (100 Hz) electric field. Further field-dependent relaxation dynamics are measured, and shown in Fig. 9, for emphasizing the specific cooperativity (in either translation or rotation) of GO-complexes. The results above (in Figs. 6 and 7) are performed by polarized light (VV-mode) scatterings, depicting mainly translational motions of GO. However, when the system contains any rotational motions, there are depolarized light (VH-mode) scattering signals that are expected to occur. Indeed, such depolarized light scattering signals are detected for two particular GO-complex mixtures; one is the GO-nafion and the other is GO-PPs-(iso) fdVs, shown in Fig. 9(b) and 9(d), respectively. Moreover, clearly additional rotational degrees of motions for the GO-complex are carried out, with showing high signal-to-noise ratios in the correlation functions, performed by depolarized (VH-mode) light scatterings. This implies then the fact somewhat membrane-structures (of both nafion and DNA-virus suspension) are capable for adapting the rotational motions of GO and the GO-complexes, under a given low AC electric field. Thus, *the most interesting result of the above is the feasibility of GO cooperativity,*

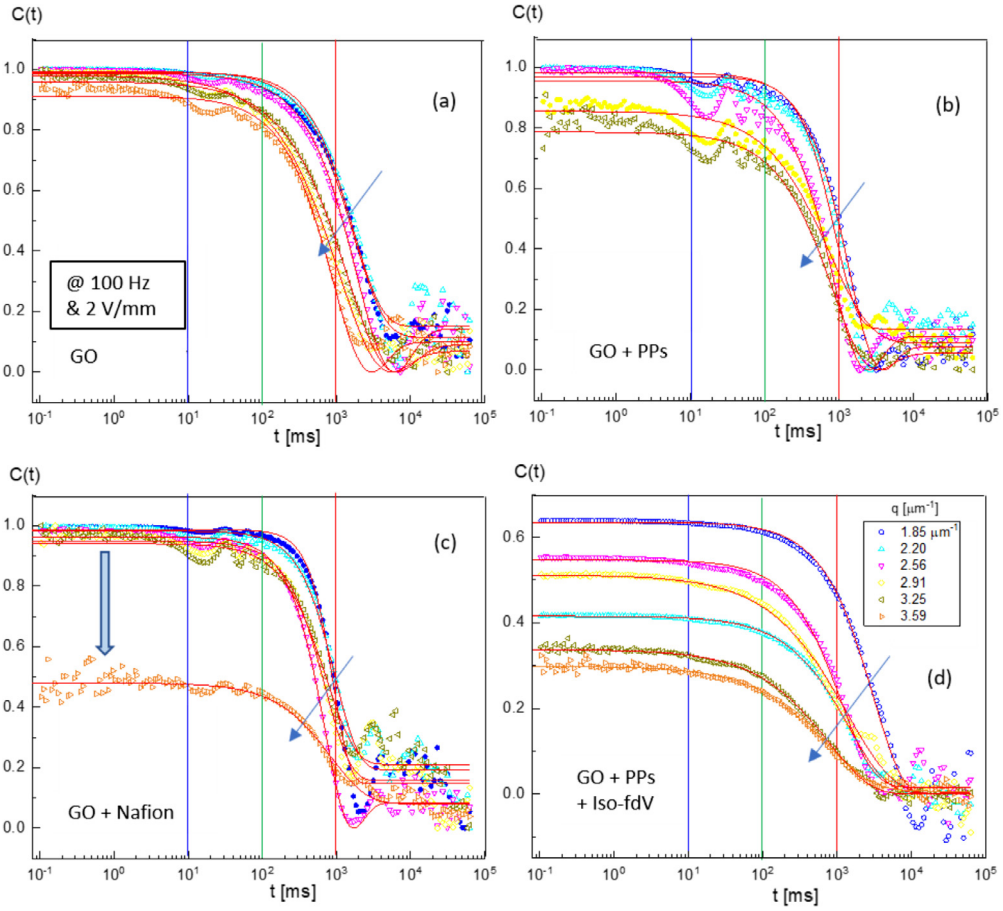

Fig. 7. The same with Fig. 6, in the case of presence of a weak electric field (of the AC field amplitude of 2 V/mm and a frequency of 100 Hz). Local oscillations are still observed for the diluted GO, the mixture of GO-PPs and GO-Nafion (in a-c), but "overdamped" in the GO-PPs-(iso) fdVs (in d). Overall, in the presence of an electric-field, well-dispersed correlation functions are obtained, in the case of the GO-PPs-(iso) fdVs in (d), compared to the absence of an electric field (in Fig. 6(d)).

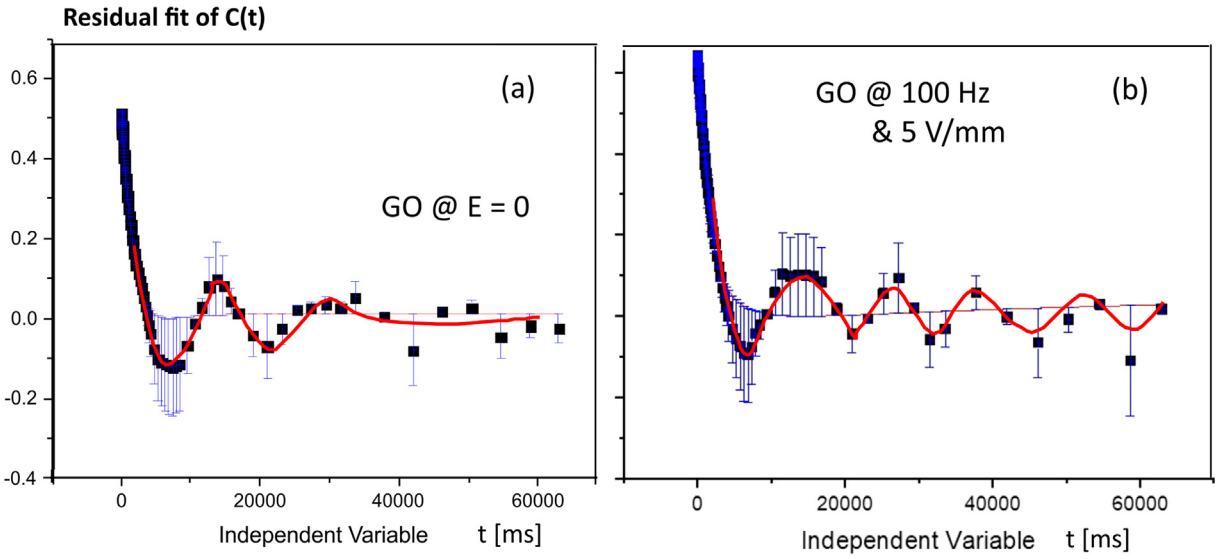

Fig. 8. The residual fit for the comparison of an intensity auto-correlation function, measured for the suspension of a diluted GO: (a) without electric field, and (b) with the field amplitude of 5 V/mm and the frequency of 100 Hz. Notably well-behaved multiple oscillations are induced as the electric field response (right), compared to the absence of a field (left).

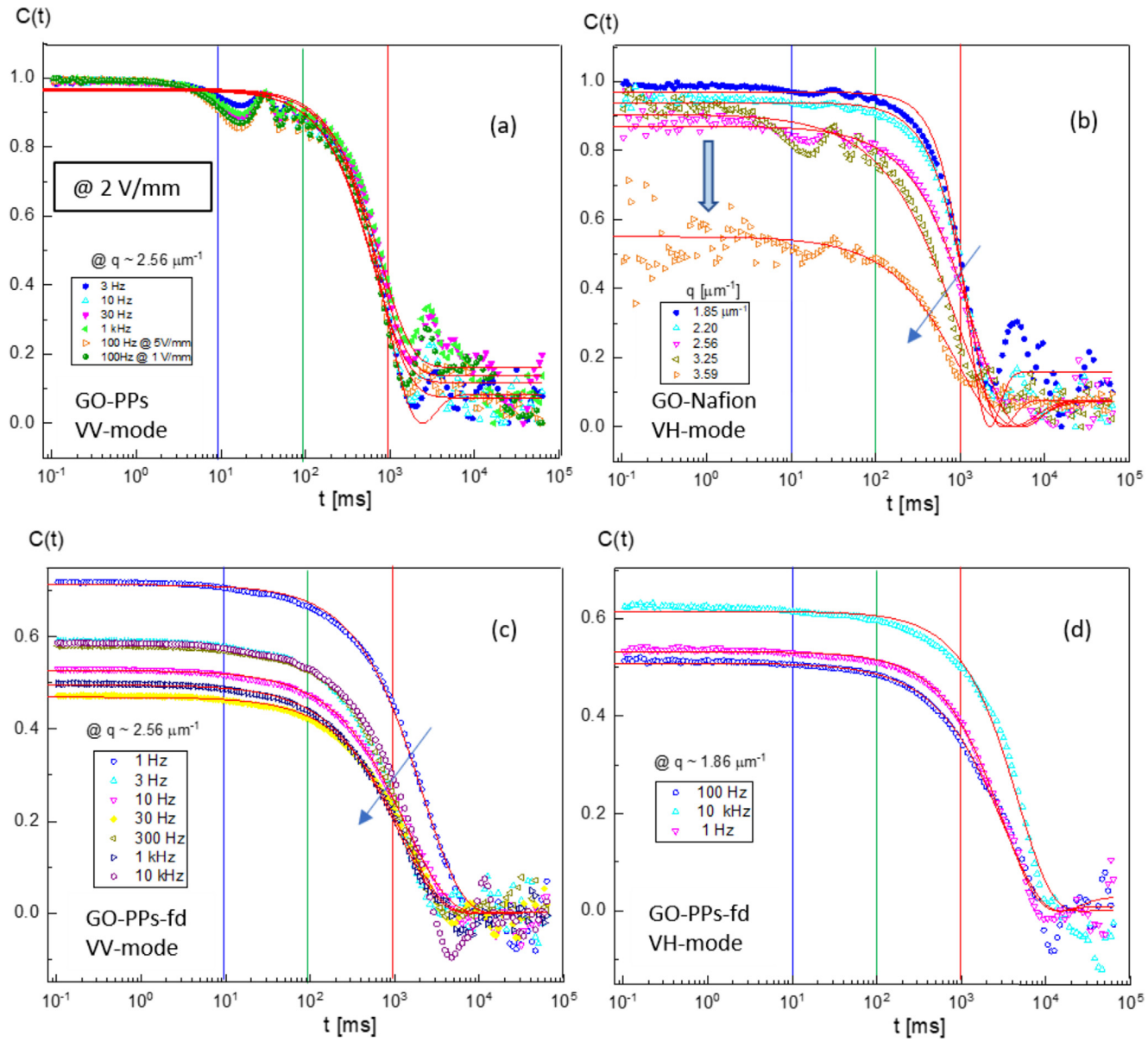

Fig. 9. Electric-field induced cooperativity in the polarized- (VV-mode) versus depolarized-light (VH-mode) scatterings of GO-complex mixtures: (a) Polarized light scattering of GO-PPs mixture at q ~ 2.56 /μm in the various field frequencies and amplitudes. (b) Depolarized light scattering of GO-Nafion mixture at various wavevectors, where the arrow indicates an increase of the wavevector. (c) Polarized light scattering of GO-PPs-(iso) fdVs mixture at q ~ 2.56 /μm for various field frequencies. (d) Depolarized light scattering of GO-PPs-(iso) fdVs mixture at q ~ 1.86 /μm for various field frequencies.

Table 1
Relaxation rates of GO-complex mixtures in low AC electric field @ 2 V/mm.

Γ [s^{-1}] q [μm^{-1}]	GO E = 0	100 Hz	GO + PPs E = 0	100 Hz	GO + Nafion E = 0	100 Hz	GO + PPs + DNA E = 0	100 Hz
1.85	0.439	0.4191	0.1273	0.35331	1.08	0.92543	0.17863	0.1598
2.20	0.4882	0.45126	0.23093	0.92	1.56	0.8428	0.2963	0.33031
2.56	0.18391	0.2078	0.4199	0.54	1.09	0.75666	0.53787	0.53788
2.91	0.64063	0.31005	0.30482	0.8453	2.07	1.11	0.27752	0.27752
3.25	0.18181	0.2398	0.12891	0.47904	1.85	1.07	0.49569	0.49569
3.59	0.21145	0.45523			2.24	0.8377	0.6829	0.6829

shown in both translation and rotation, by the open mesh-network of isotropic DNA-viruses. Such uniquely "overdamped" Brownian motions in the membrane-based environment are even distinguished by the GO-Nafion (that not as overdamped motion), in Fig. 9(c) and 9(d), respectively.

5. Conclusion

In this work, we provide the frequency-dependent orientational dynamics of GO- and GO-complexes under an influence of low AC electric fields, by means of image-time correlation spectroscopy and small angle dynamic light scattering. Fundamentally, different orientation responses of frequency-controlled rotations of GO are observed. Image-time correlations on the Fourier transformed images have demonstrated (in spatial averages) that the rotational dynamics of a GO-sheet is faster at a low frequency (100 Hz and in the absence of a field), than those at a high frequency (1 kHz). The reason for that at a high-frequency is due to the orientational response time as too large to the apparent reorientation. On the contrary, at low frequencies (<100 Hz), the GO-sheets exhibit pronounced reorientation and undergo broader distributions of different orientations, resulting a large-amplitude recovery of the image-time correlation function (as can be seen, after 20 s in Fig. 5 (c)). Such low-frequency driven feedbacks of GO are agreed well with our observed microscopic relaxation dynamics, also supported independently, by an *in-situ* electric field small angle dynamic light scattering. Furthermore, localized oscillations (in the range of 10–100 Hz), in the scattered intensity correlation functions, confirm that the occurrence of rotational motion of GO-sheets as the consequence of low-frequency feedbacks. Here, among the GO-complexes, the most prominent oscillations of GO are occurred in the mixture with polystyrene particles, due to a strong repulsive interaction between GO and PPs sphere. Other GO-complexes (under an electric field) reveal indications of localized oscillations (at low frequencies of the applied electric field) with polystyrene particles and nafion solution. *However, localized oscillations are clearly absent for the GO-sheets, in the mixture of isotropic suspension of DNA-virus and the GO-PPs, as the overdamped Brownian motion, showing no indication of oscillations.* This supports positively that the GO is stabilized cooperatively in the membrane-based networks (i.e. an isotropic rod-mesh network of DNA-suspension), immobilizing their own random rotational motion. Thus, the features of tuning ability of GO by rotational motion and their translational mobility are useful to implement externally field-induced GO-complexes (under a low-frequency of 10–100 Hz, in the electric field). In particular, the localized oscillations (with an "enhanced" GO-PPs mixture) and "overdamped" motions (by the DNA-suspension with the GO-PPs mixture), can be employed to tailor potential templates as "switchable" feedbacks of GO. As follow-up, how the GO interpenetrates into the open DNA-rod mesh network, as well the "interfacial" polarization of individual GO-sheets in the phase boundaries of rod-DNA strands can be further explored. Finally, we hope this work contributes to the potential applications of biomedical devices based on GO-related soft templates using a low AC electric field.

Author Contributions

D.L prepared and characterized the GO samples. K.K conducted the integrated experiments. K.K. and J.S organized the study. K.K, D. L. and J.S wrote the manuscript. All authors commented on the manuscript. All authors have given approval to the final version of the manuscript.

Declaration of Competing Interest

The authors declare that they have no known competing financial interests or personal relationships that could have appeared to influence the work reported in this paper.

Appendix A. Supplementary material

Supplementary data to this article can be found online at https://doi.org/10.1016/j.molliq.2021.116151.

References

[1] D.P. DiVincenzo, E.J. Mele, Self-consistent effective-mass theory for intralayer screening in graphite intercalation compounds, Phys. Rev. B 29 (1984) 1685–1694.
[2] S. Das Sarma, E.H. Hwang, Collective modes of the massless dirac plasma, Phys. Rev. Lett. 102 (2009) 206412.
[3] A.K. Geim, K.S. Novoselov, The rise of graphene, Nat. Mater. 6 (2007) 183–191.
[4] F. Bonaccorso, L. Colombo, G. Yu, M. Stoller, V. Tozzini, A.C. Ferrari, R.S. Ruoff, V. Pellegrini, Graphene, related two-dimensional crystals, and hybrid systems for energy conversion and storage, Science 347 (2015) 1246501.
[5] B.C. Brodie, XIII. On the Atomic Weight of Graphite. Philos. Trans. Royal Soc. 1859, 149, 249-259.
[6] D.W. Lee, V.L. De Los Santos, J.W. Seo, L.L. Felix, D.A. Bustamante, J.M. Cole, C.H. W. Barnes, The Structure of Graphite Oxide: Investigation of Its Surface Chemical Groups. J. Phys. Chem. B 2010, 114, 5723–5728.
[7] Z.U. Abideen, H.W. Kim, S.S. Kim, An ultra-sensitive hydrogen gas sensor using reduced graphene oxide-loaded Zno nanofibers, ChemComm 51 (2015) 15418–15421.
[8] Y. Wang, L. Zhang, N. Hu, Y. Wang, Y. Zhang, Z. Zhou, Y. Liu, S. Shen, C. Peng, Ammonia gas sensors based on chemically reduced graphene oxide sheets self-assembled on au electrodes, Nanoscale Res. Lett. 9 (2014) 251.
[9] D. Lee, J. Seo, X. Zhu, J.M. Cole, H. Su, Magnetism in graphene oxide induced by epoxy groups, Appl. Phys. Lett. 106 (2015) 172402.
[10] D. Lee, J. Seo, X. Zhu, J. Lee, H.-J. Shin, J.M. Cole, T. Shin, J. Lee, H. Lee, H. Su, Quantum confinement-induced tunable exciton states in graphene oxide, Sci. Rep. 3 (2013) 2250.
[11] D. Lee, J. Seo, Three-dimensionally networked graphene hydroxide with giant pores and its application in supercapacitors, Sci. Rep. 4 (2014) 7419.
[12] D. Lee, J. Seo, Magnetic frustration of graphite oxide, Sci. Rep. 7 (2017) 44690.
[13] H.J. Yoon, D.H. Jun, J.H. Yang, Z. Zhou, S.S. Yang, M.M.-C. Cheng, Carbon dioxide gas sensor using a graphene sheet, Sens. Actuator B-Chem. 157 (2011) 310–313.
[14] S. Deng, V. Tjoa, H.M. Fan, H.R. Tan, D.C. Sayle, M. Olivo, S. Mhaisalkar, J. Wei, C. H. Sow, Reduced graphene oxide conjugated Cu2o nanowire mesocrystals for high-performance No2 gas sensor, J. Am. Chem. Soc. 134 (2012) 4905–4917.
[15] F. Bonaccorso, Z. Sun, T. Hasan, A.C. Ferrari, Graphene photonics and optoelectronics, Nat. Photonics 4 (2010) 611–622.
[16] S. Kim, S. Zhou, Y. Hu, M. Acik, Y.J. Chabal, C. Berger, W. de Heer, A. Bongiorno, E. Riedo, Room-temperature metastability of multilayer graphene oxide films, Nat. Mater. 11 (2012) 544–549.
[17] K. Erickson, R. Erni, Z. Lee, N. Alem, W. Gannett, A. Zettl, Determination of the local chemical structure of graphene oxide and reduced graphene oxide, Adv. Mater. 22 (2010) 4467–4472.
[18] D.W. Lee, J.W. Seo, Sp2/Sp3 carbon ratio in graphite oxide with different preparation times, J. Phys. Chem. C. 115 (2011) 2705–2708.
[19] D.W. Lee, J.W. Seo, Formation of phenol groups in hydrated graphite oxide, J. Phys. Chem. C. 115 (2011) 12483–12486.
[20] T.-F. Yeh, W.-L. Huang, C.-J. Chung, I.T. Chiang, L.-C. Chen, H.-Y. Chang, W.-C. Su, C. Cheng, S.-J. Chen, H. Teng, Elucidating quantum confinement in graphene oxide dots based on excitation-wavelength-independent photoluminescence, J. Phys. Chem. Lett. 7 (2016) 2087–2092.
[21] Y. Dong, J. Shao, C. Chen, H. Li, R. Wang, Y. Chi, X. Lin, G. Chen, Blue luminescent graphene quantum dots and graphene oxide prepared by tuning the carbonization degree of citric ACID, Carbon 50 (2012) 4738–4743.
[22] J. Kim, L.J. Cote, F. Kim, W. Yuan, K.R. Shull, J. Huang, Graphene Oxide Sheets at Interfaces, J. Am. Chem. Soc. 132 (2010) 8180–8186.
[23] X. Qi, K.-Y. Pu, H. Li, X. Zhou, S. Wu, Q.-L. Fan, B. Liu, F. Boey, W. Huang, H. Zhang, Amphiphilic graphene composites, Angew. Chem. Int. Ed. 49 (2010) 9426–9429.
[24] Lee, D. W.; Seo, J. W.; Jelbert, G. R.; V., L. d. L. S.; Cole, J. M.; Panagopoulos, C.; Barnes, C. H. W., Transparent and Flexible Polymerized Graphite Oxide Thin Film with Frequency-Dependent Dielectric Constant. Appl. Phys. Lett. 2009, 95, 172901.
[25] R. Narayan, J.E. Kim, J.Y. Kim, K.E. Lee, S.O. Kim, Graphene oxide liquid crystals: discovery, evolution and applications, Adv. Mater. 28 (2016) 3045–3068.
[26] J.E. Kim, T.H. Han, S.H. Lee, J.Y. Kim, C.W. Ahn, J.M. Yun, S.O. Kim, Graphene oxide liquid crystals, Angew. Chem. Int. Ed. 50 (2011) 3043–3047.
[27] R. Basu, D. Kinnamon, A. Garvey, Nano-electromechanical rotation of graphene and giant enhancement in dielectric anisotropy in a liquid crystal, Appl. Phys. Lett. 106 (2015) 201909.
[28] W. Tie, S.S. Bhattacharyya, Y.J. Lim, S.W. Lee, T.H. Lee, Y.H. Lee, S.H. Lee, Dynamic electro-optic response of graphene/graphitic flakes in nematic liquid crystals, Opt. Express 21 (2013) 19867–19879.
[29] J. Zhang, S. Seyedin, Z. Gu, N. Salim, X. Wang, J.M. Razal, Liquid crystals of graphene oxide: a route towards solution-based processing and applications, Part. Part. Syst. Charact. 34 (2017) 1600396.
[30] J. Liu, L. Cui, D. Losic, Graphene and graphene oxide as new nanocarriers for drug delivery applications, Acta Biomater. 9 (2013) 9243–9257.

[31] B. Konkena, S. Vasudevan, Understanding aqueous dispersibility of graphene oxide and reduced graphene oxide through Pka measurements, J. Phys. Chem. Lett. 3 (2012) 867–872.
[32] X. Sun, Z. Liu, K. Welsher, J.T. Robinson, A. Goodwin, S. Zaric, H. Dai, Nano-graphene oxide for cellular imaging and drug delivery, Nano Res. 1 (2008) 203–212.
[33] L. Zhang, J. Xia, Q. Zhao, L. Liu, Z. Zhang, Functional graphene oxide as a nanocarrier for controlled loading and targeted delivery of mixed anticancer drugs, Small 6 (2010) 537–544.
[34] J-L. Dejardin, Dynamic Kerr Effect: The use and limits of the Smoluchowski equation and nonlinear inertial responses", World scientific series in contemporary chemical physics -Vol. 7, World Scientific Publishing Co. Pte. Ltd, 1995.
[35] K. Kang, Image time-correlation, dynamic light scattering, and birefringence for the study of the response of anisometric colloids to external fields, Rev. Sci. Instrum. 82 (2011) 053903.
[36] Y.D. Liu, B.J. Park, Y.H. Kim, Kim, H. J. Choi, Smart monodisperse polystyrene/polyaniline core–shell structured hybrid microspheres fabricated by a controlled releasing technique and their electro-responsive characteristics, J. Mater. Chem. 2011, 21, 17396.
[37] K. Zimmerman, J. Hagedorn, C.C. Heuck, M. Hinrichsen, J. Ludwig, The Ionic Properties of the Filamentous Bacteriophages Pf1 and Fd, J. Biol. Chem. 261 (1986) 1653.
[38] K. Kang, J.K.G. Dhont, Electric-field induced transitions in suspensions of charged colloidal rods, Soft Matter 6 (2010) 273–286.
[39] K. Kang, Electric-field induced microdynamics of charged rods" in Frontiers in Physics. 2014, Vol. 2, Article 73, doi: 10.3389/fphy.2014.00073.
[40] K. Kang, J.K.G. Dhont, An electric-field induced dynamical state in dispersions of highly charged colloidal rods: comparison of experiment and theory, Colloid Polym. Sci. 293 (2015) 3325–3336.
[41] K, Kang, J.K.G. Dhont, Structural arrest and texture dynamics in suspensions of charged colloidal rods, Soft Matter, 2013, 9, 4401.
[42] K. Kang, S.H. Piao, H.J. Choi, Synchronized oscillations of dimers in biphasic charged fd-virus suspensions, Phys. Rev. E. 94 (2016) 020602(R).
[43] K. Kang, J.S. Hong, J.K.G. Dhont, Local interfacial migration of clay particles within an oil droplet in an aqueous environment, J. Phys. Chem. C. 118 (2014) 24803–24810.
[44] Z.-T. Zhang, X. Zha, B.-Y. Cao, Diffusion tensors of arbitrary-shaped nanoparticles in fluid by molecular dynamics simulation, Sci. Rep. 9 (2019) 18943.
[45] B.-Y. Cao, R.-Y. Dong, Molecular dynamics calculation of rotational diffusion coefficient of a carbon nanotube in fluid, J. Chem. Phys. 140 (2014) 034703.
[46] J. Zhang, G.J. Weng, X. Xia, C. Fang, A theory of frequency dependence and sustained high dielectric constant in functionalized graphene-polymer nanocomposites, Mech. Mater. 144 (May 2020) 103352.
[47] X. Xia, Y. Wang, Z. Zhong, G.J. Weng, A frequency-dependent theory of electrical conductivity and dielectric permittivity for graphene-polymer nanocomposites, Carbon 111 (2017) 221–230.
[48] J.K.G. Dhont, Kang, K, Electric-field–induced polarization of the layer of condensed ions on cylindrical colloids, Eur. Phys. J. E. 34 (2011) 40.